ELSEVIER

Long-wave radiative analysis of cloudy scattering atmospheres using a net exchange formulation

V. Eymet[a,*], J.L. Dufresne[b], P. Ricchiazzi[c], R. Fournier[a], S. Blanco[a]

[a] *Laboratoire d'Energétique, UFR-PCA, Université Paul Sabatier, 118 route de Narbonne, 31062 Toulouse cedex, France*
[b] *LMD/CNRS, Université de Paris VI, 75252 Paris, France*
[c] *Institute for Computational Earth System Science, University of California at Santa Barbara, Santa Barbara, CA, USA*

Abstract

The Net Exchange Formulation (NEF) is an alternative to the usual radiative transfer equation. It was proposed in 1967 by Green [Q. J. R. Meteorol. Soc. 93 (1967) 371] for atmospheric sciences and by Hottel [H.C. Hottel, A.F. Sarofim. Radiative Transfer McGraw Hill, New York, 1967] for engineering sciences. Until now, the NEF has been used only in a very few cases for atmospheric studies. Recently we have developed a long-wave radiative code based on this formulation for a GCM of the Mars planet. Here, we will present results for the Earth atmosphere, obtained with a Monte Carlo Method based on the NEF. In this method, fluxes are not addressed any more. The basic variables are the net exchange rates (NER) between each pair of atmospheric layer (i, j), i.e. the radiative power emitted by i and absorbed by j minus the radiative power emitted by j and absorbed by i. The graphical representation of the NER matrix highlights the radiative exchanges that dominate the radiative budget of the atmosphere and allows one to have a very good insight of the radiative exchanges. Results will be presented for clear sky atmospheres with Mid-Latitude Summer and Sub-Arctic Winter temperature profiles, and for the same atmospheres with three different types of clouds. The effect of scattering on long-wave radiative exchanges will also be analysed.
© 2004 Elsevier B.V. All rights reserved.

* Corresponding author. Tel.: +33-5-61-55-60-04; fax: +33-5-61-55-60-21.
E-mail address: eymet@energetique.ups-tlse.fr (V. Eymet).

1. Introduction

The Net Exchange Formulation (NEF) is an alternative to the usual radiative transfer formulation. It was proposed by Green, 1967 for atmospheric sciences and by Hottel and Sarofim, 1967 for engineering sciences. Joseph and Bursztyn, 1976 attempted to use this approach to model radiative transfer in the terrestrial atmosphere. They showed that radiative net-exchanges between an atmospheric layer and the boundaries (space and ground) are dominant and that net-exchanges with the rest of the atmosphere contribute to around 15% of the total energy budget, but they encountered some numerical difficulties. Stephens, 1984 also presented this formalism in his review paper but to date the NEF is not commonly used for atmospheric studies.

The long-wave radiative code represents a very significant part of the computer time requirements of most GCMs and some important simplifications have to be performed. For instance, LW radiative codes are often called at lower frequencies than the rest of the physics, although some key variables (humidity, clouds, etc.) may change significantly from one time step to the next. Another example: most LW radiative codes neglect the effects of scattering by cloud water droplets and/or large aerosols although some studies have suggested that this approximation may lead to nonnegligible errors (for instance Edwards and Slingo, 1996; Dufresne et al., 2002). Even if scattering can be considered by some codes, this possibility is commonly turned off in order to save CPU time Lacis and Mishchenko, 1995.

The purpose of this paper is to show that the NEF may be a good framework to get some useful insight into radiative transfer within the atmosphere, particularly for identification of the radiative exchanges that contributes the most to atmospheric heating rates. In the long term, on the basis of such analysis, our final goal is to develop a NEF parameterization of the effects of scattering in the LW. We will make a short presentation of the formalism and of the Monte-Carlo Method that we have developed (Section 2). The choice of a Monte-Carlo Method was motivated by its high flexibility. We will present some analysis for clear sky atmospheres (Section 3) and for cloudy atmospheres (Section 4) through which we further illustrate and quantify some lassical results. Finally, we will analyze how scattering may affect radiative exchanges in cloudy atmospheres (Section 5).

2. Net exchange formulation and Monte-Carlo method

Most numerical methods for solving long-wave atmospheric radiative transfer are based on the integro-differential form of the radiative transfer equation. Using the Net Exchange Formulation (NEF) based on Net Exchange Rates (NER) as first proposed by Green (1967) may represent a very interesting alternative. In terms of physical images, the NEF allows a complete decomposition of net radiative budgets as sums of NERs between each atmospheric layer and ground, space, and the rest of the atmosphere. An application similar to the present one (using a NEF toward radiative transfer parameterization in a GCM) was the subject of a previous work concerning the Martian atmosphere (Dufresne et al., submitted for publication). Cooling to space is known to be the dominant term of the cooling rate and the "cool to space" approximation has first been proposed by Rodgers
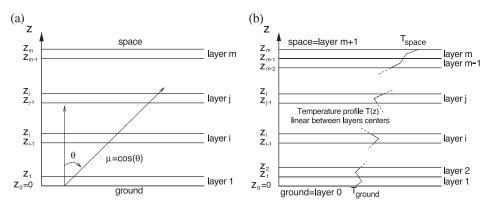
Fig. 1. (a) Classical discretization of 1-D inhomogeneous atmosphere into m homogeneous atmospheric layers; (b) atmospheric configuration used for radiative transfer computations.

and Walshaw, 1966. Dividing the cooling rate into a ''cooling to space'' term and an ''exchange'' term allows to build fast and precise algorithms (Fels and Schwarzkopf, 1975; Schwarzkopf and Fels, 1991). Here we go further and we gather the cooling rate in individual exchange terms between each pair of layer of the atmosphere.

The Net Exchange Rate between two arbitrary elements i and j (either volume or surface elements) is defined as the energy rate emitted from element i and absorbed by j, minus energy rate emitted from j and absorbed by i. In the very general case of an inhomogeneous absorbing and scattering medium, NER have been formulated in a previous article (Eymet et al., 2004). In the case of a one-dimensional atmospheric radiative transfer calculation (see Fig. 1(a)), expressing the monochromatic NER $\Psi_{ij,v}$ between two arbitrary atmospheric layers i and j is straight forward, as illustrated below:

$$
\Psi_{ij,v} = \int_{2\pi} d\Omega \int_{z_{i-1}}^{z_i} \frac{dz}{\mu} \int_{z_{j-1}}^{z_j} \frac{dz'}{\mu} \mu \kappa_{a,v}(z) \kappa_{a,v}(z')
$$

$$
\times (B_v(z) - B_v(z')) \exp\left(-\int_z^{z'} \frac{\kappa_{a,v}(z'')}{\mu} dz''\right) \tag{1}
$$

As this expression makes clear, if layer i is warmer than layer j, $\Psi_{ij,v}$ is the rate at which layer i is cooled by all radiative interactions with layer j (and reciprocally, the rate at which j is warmed by interactions with i).

Similarly, the monochromatic NER $\Psi_{ig,v}$ and $\Psi_{is,v}$ respectively between layer i and the ground, and between layer i and space, are given below for purely absorbing atmospheres:

$$
\Psi_{ig,v} = \int_{2\pi} d\Omega \int_{z_{i-1}}^{z_i} \frac{dz}{\mu} \mu \kappa_{a,v}(z)(B_v(z) - B_v(\text{ground})) \exp\left(-\int_0^z \frac{\kappa_{a,v}(z')}{\mu} dz'\right) \tag{2}
$$

$$
\Psi_{is,v} = \int_{2\pi} d\Omega \int_{z_{i-1}}^{z_i} \frac{dz}{\mu} \mu \kappa_{a,v}(z)(B_v(z) - B_v(\text{space})) \exp\left(-\int_z^H \frac{\kappa_{a,v}(z')}{\mu} dz'\right) \tag{3}
$$

z_i represents the top altitude of layer i, $k_{a,v}(z)$ is the monochromatic absorption coefficient at altitude z, and $B_v(z)$ is the monochromatic blackbody intensity at altitude z. Also, $d\Omega = \sin(\theta)d\theta d\phi$, with θ and ϕ being the classical spherical coordinates.

Still for illustration purposes, with the assumption of a uniform temperature profile within each atmospheric layer, Eq. (1) reduces to:

$$\Psi_{ij,v} = \xi_{ij,v}(B_v(i) - B_v(j)) \tag{4}$$

where $B_v(i)$ and $B_v(j)$ are monochromatic blackbody intensities in layers i and j. $\xi_{ij,v}$ is a monochromatic optico-geometric factor. With the assumption of a purely absorbing media, let $\tau_{i,j,v}$ be the monochromatic transmittivity between z_i and z_j; $\xi_{ij,v}$ may then be expressed as a function of these monochromatic transmittivities:

$$\xi_{i,j,v} = \tau_{i,j-1,v} - \tau_{i-1,j-1,v} - \tau_{i,j,v} + \tau_{i-1,j,v} \tag{5}$$

Considering Eq. (5), it is easy to see that $\xi_{ij,v} > 0$; thus, the sign of $\Psi_{ij,v}$ depends only on the sign of $B_v(i) - B_v(j)$ (still within the limits of the assumptions of a uniform temperature profile across each atmospheric layer and of a purely absorbing media).

During the last few years, a series of articles (Cherkaoui et al., 1996; Cherkaoui et al., 1998; Tessé et al., 2002) have investigated use of the NEF within a Monte Carlo Framework. NEF based Monte-Carlo algorithms have been improved in terms of sampling laws adjustment in order to bypass various numerical convergence difficulties encountered in quasi-isothermal configurations (Cherkaoui et al., 1996), purely absorbing optically thick media (De Lataillade et al., 2002a) and both absorbing and scattering optically thick media (Eymet et al., 2004).

For the present study, the choice of using a Monte-Carlo Method for computing NERs was mainly motivated by its high flexibility. In particular, the Monte-Carlo Method (MCM) is one of the numerical methods that can be easily adapted to perform NER computations.[1] Another main advantage of the MCM is its ability to compute, in addition to each radiative transfer quantity, a numerical uncertainty over this result (in fact, the statistical standard deviation), which makes the MCM a reference method. Finally, it has recently been shown (De Lataillade et al., 2002b) that sensitivities of any quantity to any parameter of the problem could be computed using the MCM with very low extra computing costs.

This paper is not intended to provide new theoretical developments concerning Monte-Carlo numerical algorithms. The results shown in the rest of this article have been obtained using the Monte-Carlo algorithm presented in by Eymet et al. (2004), for the particular case of the long-wave radiative transfer in the Earth's atmosphere. Algorithmic details, and especially the methodological developments that allowed the development of an efficient algorithm to address Earth atmospheric radiation in the whole IR range (despite of the difficulties encountered by standard MCM at high optical thicknesses), can be found in the above references. The purpose of this paper is to present long-wave radiative transfer computation results in some common terrestrial configurations, and to analyze these results with the emphasis on the effect of scattering by water and ice clouds.

---

[1] This is the case of all methods based on an integral form of the Radiative Transfer Equation, but differential methods are generally not adapted to NER evaluations.

The configuration is represented in Fig. 1(b). The inhomogeneous terrestrial atmosphere is divided into m gaseous layers with homogeneous gas constituent concentrations, thus homogeneous optical properties (absorption coefficient k_a, scattering coefficient k_d, single scattering albedo ω, phase function asymmetry parameter g). Ground is denoted layer 0 and space is layer $m+1$. The temperature profile $T(z)$ is considered as linear between layers centers. Temperature of space is fixed at 0 K (no downward intensity from space in the long-wave spectral domain).

Computations presented in the following sections have been performed using the atmospheric radiative transfer Monte-Carlo algorithm with 10^6 statistical events per atmospheric layer, which ensures that every result has been computed with a statistical standard deviation lower than 0.1%.

3. Clear sky results

The results presented in this section have been obtained for clear sky configurations. Long-wave atmospheric optical properties are based on detailed information from the HITRAN2000 molecular line database, which contains over a million spectral lines for 36 different molecules (Rothman et al., 2003). To minimize computational expense, this information is converted into a set of correlated-k optical depths (Lacis and Hansen, 1991) at a relatively coarse spectral resolution using the SBMOD model (Yang et al., 2000). The first step in the process is to evaluate the line-by-line spectral profile within each spectral bin and for each layer in the atmosphere. Second, the profiles are sampled at a high-spectral resolution, and sorted by absorption strength, thereby providing a smooth, monotonically increasing representation of the absorption strength distribution in the spectral band. The resulting absorption-sorted profiles are then assigned into as many as 16 quadrature bins. This process is applied to each of 50 homogeneous layers in the model atmosphere. For the calculations performed here, a spectral resolution of 20 cm^{-1} was chosen to cover the spectral range between 100 and 2500 cm^{-1} (4 and 100 μm). Two standard (McClatchey et al., 1971) atmospheric profiles are used: a Mid-Latitude Summer (MLS) and a Sub-Arctic Winter (SAW) profile, with standard gaseous species concentrations.

3.1. Heating rates

Figs. 2(a) and 3(a) show heating rates in K/day integrated over the long-wave spectral region for the MLS and SAW clear sky configurations. These results are comparable to results already published (Fu et al., 1997; Li and Fu, 2000). The heating rate in layer i, denoted χ_i, may be interpreted as a sum of net exchanges, χ_{ij}:

$$\chi_{ij} = \frac{g}{C_p} \frac{1}{\delta t} \frac{\Psi_{ij}}{\delta p_i} \qquad (6)$$

where g is the gravity, C_p is the heat capacity of air at constant pressure, δt the length of the day, δp_i the pressure difference between the top and the bottom of layer i, and ψ_{ij} the NER

(a) MLS clear sky heating rate
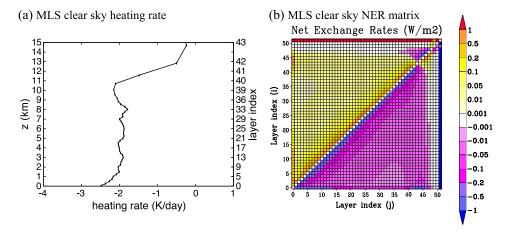
(b) MLS clear sky NER matrix

Fig. 2. (a) Heating rate (K/day) for a clear sky MLS atmospheric profile, represented between ground and an altitude of 15 km. (b) Frequency integrated NERs (W/m^2) for the same atmospheric profile. The color of the square identified by layers numbers i and j represents the Net Exchange Rate between layers i and j. Layer 0 is the ground and layer 51 represents space.

between layers i and j (Table 1). Within this framework, the total heating rate of layer i is:

$$\chi_i = \sum_j \chi_{ij} \tag{7}$$

Of course, heating rates χ_i may also be computed from $\Psi_i = \Sigma_j \Psi_{ij}$ the total radiative budget of layer i:

$$\chi_i = \frac{g}{C_p} \frac{1}{\delta t} \frac{\Psi_i}{\delta p_i} \tag{8}$$

The fact that individual heating rates may be interpreted as a sum of NER allows a complete decomposition of these heating rates; in particular, this decomposition may, for instance, lead to the conclusion that the heating rate of a given layer i is mainly driven by a small number of clearly identified NERs, and that the contribution of all others NERs is negligible.

3.2. Net Exchange Rate matrices

Figs. 2(b) and 3(b) show the Net Exchange Rates matrices (integrated over the long-wave spectral region) in W/m^2. Each element of the matrix displays the intensity of the net exchange rate Ψ_{ij} between each pair (i,j) of atmospheric layers. As an example of reading Fig. 2(b), consider layer $i = 10$. The horizontal line of the matrix for layer 10 shows the decomposition of the heating rate in layer 10 in terms of NER contributions. Layer 10 is for instance heated by the ground (layer 0) and underlying warmer gas layers, and loses

Table 1
Top altitudes of atmospheric G.C.M. layers used in the vertical discretization

Layer index	Top altitude (km)	Layer index	Top altitude (km)
1	0.125	26	6.375
2	0.375	27	6.625
3	0.625	28	6.876
4	0.875	29	7.126
5	1.125	30	7.378
6	1.375	31	7.632
7	1.625	32	7.888
8	1.875	33	8.149
9	2.125	34	8.419
10	2.375	35	8.704
11	2.625	36	9.016
12	2.875	37	9.371
13	3.125	38	9.797
14	3.375	39	10.339
15	3.625	40	11.069
16	3.875	41	12.094
17	4.125	42	13.584
18	4.375	43	15.795
19	4.625	44	19.113
20	4.875	45	24.114
21	5.125	46	31.648
22	5.375	47	42.964
23	5.625	48	59.876
24	5.875	49	85.000
25	6.125	50	100.000

energy toward the colder layers above and toward space. Of course the matrix is antisymmetric because $\Psi_{ji} = -\Psi_{ij}$. Diagonal terms are null because there is no net exchange between a given layer and itself.

(a) SAW clear sky heating rate
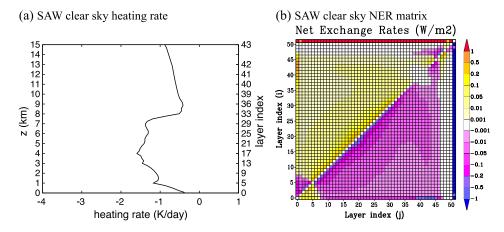
(b) SAW clear sky NER matrix

Fig. 3. Same as Fig. 2 for Sub-Arctic Winter atmospheric profile.

In Fig. 2(b), dominant terms are net exchanges between each atmospheric layer and the ground (first row and first column), each atmospheric layer and space (last row and last column), and also between close atmospheric layers (close to diagonal terms). Note an NER sign inversion in stratospheric layers: for instance, layer 45 is heated by warmer layers 0–41. However, layer 45 is also cooled from below by layers 42–44, and heated from above by layers 46–48. This is due to an MLS temperature profile inversion in the stratosphere.

Conclusions are similar for the SAW clear-sky configuration (Fig. 3(a)), except that two temperature inversions are noticeable: the first at ≈ 1-km altitude, and the second at ≈ 42-km altitude. These inversions in the temperature profile are visible in the NER matrix. Also, a group of null near diagonal terms is visible for layers 38–43. This is due to the fact that, in these layers, the temperature profile is a constant (see Fig. 4).

3.3. Spectral analysis

The heating rate at a given altitude for a clear sky configuration is mainly due to heating from ground, cooling to space and exchange with adjacent atmospheric layers. From this conclusion, the total radiative budget $\Psi_{i,v}$ for each atmospheric layer i, in each narrow-band centered around frequency v, has been decomposed into three main terms, the net exchange between atmospheric layer i and ground $\Psi_{i,v}^{\mathrm{gas-ground}}$, the net exchange between atmospheric layer i and space $\Psi_{i,v}^{\mathrm{gas-space}}$, and the net exchange between atmospheric layer i and the rest of the atmosphere $\Psi_{i,v}^{\mathrm{gas-gas}}$:

$$\Psi_{i,v} = \Psi_{i,v}^{\mathrm{gas-ground}} + \Psi_{i,v}^{\mathrm{gas-space}} + \Psi_{i,v}^{gas-gas} \tag{9}$$

Fig. 5(a) represents the total radiative budget as a function of altitude, for each spectral narrow-band of width 20 cm^{-1} between 4 and 100 μm (see Table 2 for correspondence between narrow-band index, frequency and wave numbers) and may be compared with figures previously published by Clough and Iacono, 1995. Fig. 5(b)–(d) represents the different terms of the total radiative budget: net exchange between each atmospheric layer
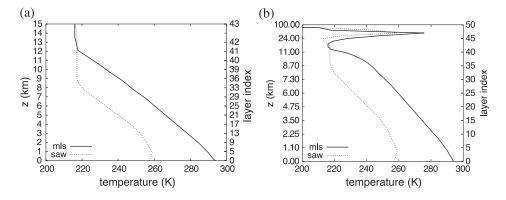

Fig. 4. Temperature profiles (K) in a McClatchey Mid-Latitude Summer (MLS) atmosphere and in a Sub-Arctic Winter (SAW) atmosphere. Scale is (a) linear with altitude and (b) linear with layer index.
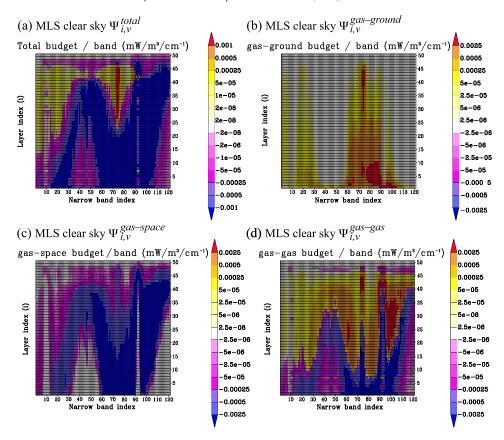
(a) MLS clear sky $\Psi_{i,v}^{total}$

Total budget / band (mW/m³/cm⁻¹)

(b) MLS clear sky $\Psi_{i,v}^{gas-ground}$

gas−ground budget / band (mW/m³/cm⁻¹)

(c) MLS clear sky $\Psi_{i,v}^{gas-space}$

gas−space budget / band (mW/m³/cm⁻¹)

(d) MLS clear sky $\Psi_{i,v}^{gas-gas}$

gas−gas budget / band (mW/m³/cm⁻¹)

Fig. 5. (a) Total radiative budget (mW/m³/cm[1]) as a function of narrow-band index (see Table 2) and atmospheric layer index, for a clear sky MLS configuration; (b) Net exchange between each atmospheric layer and ground (mW/m³/cm[1]); (c) Net exchange between each atmospheric layer and space (mW/m³/cm[1]); (b) Net exchange between each atmospheric layer and the rest of the atmosphere (mW/m³/cm[1]).

and ground, net exchange between each atmospheric layer and space, and net exchange between each atmospheric layer and the rest of the atmosphere. Fig. 6(a)–(d) is identical to Fig. 5 for a clear sky SAW configuration.

Fig. 5(b) shows that the net exchange between each atmospheric layer and ground $\Psi_{i,v}^{gas-ground}$ is positive in an MLS configuration, because the ground is heating all atmospheric layers: the ground temperature is higher than all gas temperatures. The heating effect is decreasing with altitude, because of absorption by lower atmospheric layers. The attenuation does not follow a strict exponential law, because of spectral correlations in the long-wave range. Moreover, the heating from ground is dominant in low absorption spectral regions, such as the so-called "atmospheric window" which extends from 8 to 13 μm at ground level (narrow-band index 63–82), while net exchange between ground and atmospheric layers is null in strong absorption spectral regions, such as the 15 μm CO_2 band (narrow-band index 93) and the water absorption regions (narrow-bands 30 to 60 and narrow-bands 100 to 120). In other absorption bands, such as the 9.2-

Table 2
Frequency and wave number as function of narrow-band index

Narrow-band index	Frequency (μm)	Wave number (cm^{-1})
1	4.000	2500
15	4.504	2200
26	5.000	2000
35	5.494	1820
43	6.024	1660
49	6.493	1540
55	7.042	1420
64	8.064	1240
76	10.000	1000
86	12.500	800
94	15.625	640
101	20.000	500
106	25.000	400
110	31.250	320
116	50.000	200
118	62.500	160
121	100.000	100

μm ozone band (narrow-band 72) and the 4.2-μm CO_2 band (narrow-band 10), $\psi_{i,v}^{\text{gas}-\text{ground}}$ depends on the local variation of optical thickness with altitude. In a SAW configuration (Fig. 6(b)), the temperature of gas is higher than the ground temperature in the low atmosphere (see Fig. 4). Thus, $\Psi_{i,v}^{\text{gas}-\text{ground}}$ is negative in the first 2 km (first 7 atmospheric layers); above 2 km, the gas temperature drops below the ground temperature and $\Psi_{i,v}^{\text{gas}-\text{ground}}$ is positive.

The net exchange between each atmospheric layer and space $\Psi_{i,v}^{\text{gas}-\text{space}}$ (Figs. 5(c) and 6(c)) is negative, because space is cooler than all atmospheric layers, and $\Psi_{i,v}^{\text{gas}-\text{space}}$ is dominant in spectral regions where variation of optical thickness with altitude is dominant. Net exchange between gas layers and space is only possible for layers that are "visible" from space. In low absorption spectral regions, all atmospheric layers can exchange radiation with space, while in strong absorption regions (such as water absorption bands), exchange with space is only possible for top layers.

The net exchange between each atmospheric layer and the rest of the atmosphere $\Psi_{i,v}^{\text{gas}-\text{gas}}$ (Figs. 5(d) and 6(d)) is positive for layers close to the ground, and negative for higher layers. The inversion altitude depends on the narrow-band, and is higher in strong absorption regions. $\Psi_{i,v}^{\text{gas}-\text{gas}}$ depends both on the local variation of optical thickness with altitude and on the local variation of the temperature gradient with altitude.

4. Cloudy sky results

This section presents the results of computations held for cloudy configurations, with both MLS and SAW atmospheric profiles. For each atmospheric profile, four cloudy configurations have been examined (same configurations as in Fu et al., 1997): low cloud (water cloud extending from 1.0 to 2.0 km for MLS, from 0.5 to 1.5 km for SAW, with
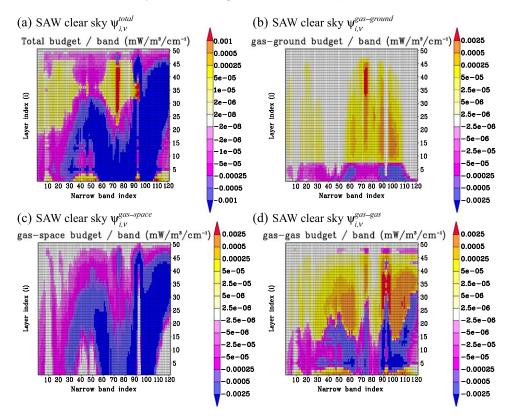
(a) SAW clear sky $\psi_{i,v}^{total}$

(b) SAW clear sky $\psi_{i,v}^{gas-ground}$

(c) SAW clear sky $\psi_{i,v}^{gas-space}$

(d) SAW clear sky $\psi_{i,v}^{gas-gas}$

Fig. 6. Same as Fig. 5 for a clear sky SAW configuration.

LWC = 0.22 g m^{-3} and effective radius r_e = 5.89 μm), middle cloud (water cloud extending from 4.0 to 5.0 km for MLS, from 2.0 to 3.0 km for SAW, with LWC = 0.28 g m^{-3} and r_e = 6.20 μm), high cloud (ice cloud extending from 10 to 12 km for MLS, from 6 to 8 km for SAW, with IWC = 0.0048 g m^{-3} and effective diameter D_e = 41.5 μm) and finally all three clouds simultaneously.

For these different configurations, this section will present NER matrices and heating rates, corresponding radiative budgets and their spectral decomposition.

4.1. NER matrices and heating rates

Figs. 7–9 present heating rates in K/day, in both (a) mid-latitude summer and (b) subarctic winter atmosphere, for cloudy configurations. Generally speaking, the bottom of all kind of clouds is heated, because the ground is warmer than the gas at cloud altitude. However, this is not true in the case of a low cloud with a SAW atmospheric profile: the bottom of the cloud is located at an altitude ≈ 1 km, which is the altitude of maximum temperature (higher than ground temperature). In all cases, the top of the cloud is cooled because of radiative exchanges with above gas layers and space, which have lower
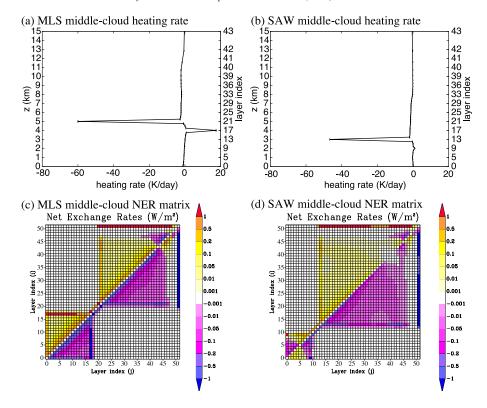
Fig. 7. (a) Heating rate (*K/day*) for MLS middle-cloud configuration (water cloud extending from 4.0 to 5.0 km (layers 17–21) with LWC=0.28 g m^{-3} and r_e=6.20 μm); (b) same as (a) for SAW atmosphere (water cloud extending from 2.0 to 3.0 km (layers 8–13) and same LWC and r_e); (c) NER matrix W/m^2) in the middle-cloud configuration for an MLS atmospheric profile; (d) same as (c) for a SAW atmospheric profile.

temperatures than the cloud. For optically thick clouds, such as a low and middle clouds in an MLS configuration, it can be seen that the middle of the cloud has a very small heating rate. In such cases, the middle layers are radiatively isolated from the rest of the system because of the high optical thickness of the cloud.

Figs. 7–9(c,d) present the NER matrices in W/m^2 for the same configurations. For low clouds (figure not shown) and middle clouds (Lacis and Mishchenko, 1995) (with visible optical depths respectively 60 and 72), it can be seen that dominant exchanges for layers located below the cloud are between each atmospheric layer and the ground, between each atmospheric layer and the bottom of the cloud, and between close atmospheric layers (near diagonal NERs); similarly, for layers located above the cloud, dominant exchanges are between each layer and space, between each layer and the top of the cloud, and also between close atmospheric layers. In these two cases, the optical thickness of the cloud is high enough so that no radiative exchange can occur between atmospheric layers located on opposites sides of the cloud. For optically thick clouds, the cloudy layer behaves as a boundary (such as ground and space). The heating rate profile gives the same quantitative
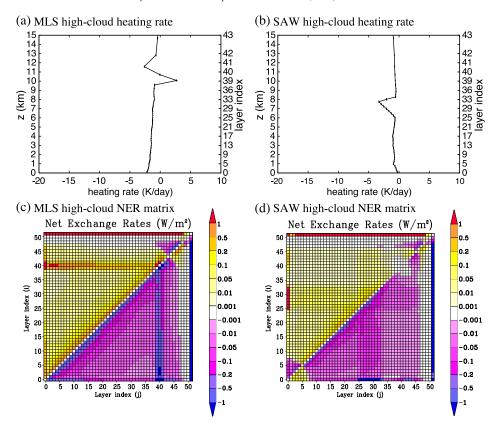
Fig. 8. (a) Heating rate (K/day) for MLS high-cloud configuration (ice cloud extending from 10.0 to 12.0 km (layers 39–41) with IWC = 0.0048 g m^{-3} and D_e = 41.5 μm); (b) same as (a) for SAW atmosphere (water cloud extending from 6.0 to 8.0 km (layers 25–33) and same IWC and D_e); (c) NER matrix (W/m^2) in the high-cloud configuration for an MLS atmospheric profile; (d) same as (c) for a SAW atmospheric profile.

result: the bottom of the cloud is heated by the ground, and the top of the cloud is cooled by space in low and middle cloud configurations.

In the case of the high cloud (Fig. 8), which is an ice cloud with a visible optical depth of approximatively 0.8, radiative exchange can occur between layers located below and above the cloud. The optical thickness of the cloud is not high enough for total extinction to occur. Dominant exchanges are between each layer and the ground, between each layer and space, between close atmospheric layers, and also between each cloud-free layer and cloudy atmospheric layers.

Finally, in the configuration where all clouds are present (Fig. 9), optically thick clouds (low and middle) behave as opaque screens, thus defining independent sections of the atmosphere which would not interact through radiation. Three main sections appear: the first, located below the low cloud; the second, between low and middle clouds; and the last, above the middle cloud. On the other hand, optically thin clouds (high clouds) allow radiative transfer between layers located below and above these clouds.
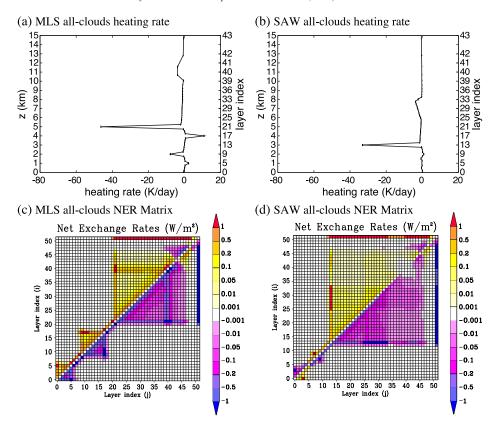
(a) MLS all-clouds heating rate

(b) SAW all-clouds heating rate

(c) MLS all-clouds NER Matrix

(d) SAW all-clouds NER Matrix

Fig. 9. (a) Heating rate (K/day) for MLS all-clouds configuration; (b) same as (a) for SAW atmosphere; (c) NER matrix (W/m^2) for an MLS all-clouds configuration; (d) same as (c), for a SAW atmosphere.

In each section of the atmosphere, dominant exchanges are between cloud-free layers and the bottom boundary (ground or top of cloud), between cloud-free layers and the top boundary (space or bottom of cloud), and between adjacent cloud-free layers or, in the specific case of high clouds, between cloud-free layers and all cloudy layers.

4.2. Spectral analysis

For clear sky configurations (see Section 3), it was chosen to present the spectral radiative budget $\psi_{i,v}^{\text{total}}$ and its three components: $\psi_{i,v}^{\text{total}} = \psi_{i,v}^{\text{gas}-\text{ground}}\} + \psi_{i,v}^{\text{gas}-\text{space}} + \psi_{i,v}^{\text{gas}-\text{gas}}$. In this section, the same decomposition of spectral radiative budgets has been kept.

NER matrix analysis in the previous section showed that optically thick clouds behave as opaque screens between layers located in either of their sides, thus dividing the atmosphere into radiatively independent sections. On the contrary, optically thin clouds behave as non-opaque screen, allowing radiative transfers between layers located below and above such clouds. These were spectrally integrated results, and this section will now

present the corresponding spectral decomposition of NERs in terms of net radiative budgets: see Fig. 10.

These figures first show that the net exchanges between each atmospheric layer and ground, in the presence of optically thick clouds (Fig. 10(b)), can occur only for layers located below the cloud, only in low absorption spectral regions. For high absorption spectral regions (such as the water or the CO_2 absorption bands), radiation emitted from the ground is totally absorbed within the first atmospheric layer, net exchanges between ground and higher layers being therefore impossible. Similarly, Fig. 10(c) shows that net exchanges between each atmospheric layer and space can occur only above optically thick clouds, in low absorption spectral regions. This confirms that optically thick clouds behave as opaque screens between the ground and space. This is true over the whole infrared spectra, but this effect is only visible in low absorption spectral regions because net exchanges between boundaries and gaseous layers are only possible in these spectral regions.
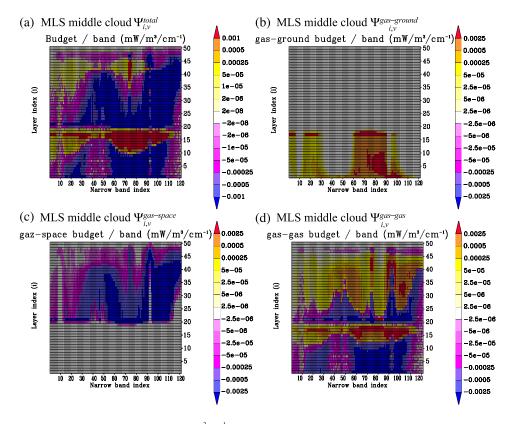

Fig. 10. (a) Total radiative budget (mW/m³/cm[1]) as a function of narrow-band index (narrow-band width = 20 cm^{−1}, from 4 to 100 μm) and atmospheric layer index, for middle cloud MLS configuration; (b) net exchange between each atmospheric layer and ground (mW/m³/cm[1]); (c) net exchange between each atmospheric layer and space (mW/m³/cm[1]); (d) net exchange between each atmospheric layer and the rest of the atmosphere.

Optically thin high clouds (figures not shown) do not behave as opaque screens: net exchanges are possible between ground and layers located above the cloud, and between space and layers located below the cloud, still for low absorption spectral regions.

5. Effects of scattering

The effects of the scattering process are generally neglected by the G.C.M. community in atmospheric long-wave radiative transfer computations. However, increasing precision requirements[2] now imply that scattering should be accounted for in G.C.M. long-wave radiative transfer schemes (Dufresne et al., 2002). Within this framework, this section will present the effect of scattering for the same cloudy configurations as used in preceding sections. First of all, the effect of scattering will be shown over ground and space total radiative budgets. Then it will be shown over previously introduced NER matrices and heating rate profiles. Finally, these results will be spectrally decomposed in order to understand which long-wave spectral ranges are affected by scattering. The results of this analysis are expected to be used in order to set up a new parameterization of long-wave radiative transfers, which accounts for scattering, in an already existing Global Circulation Model.

5.1. Effects of scattering on ground and space total radiative budgets

Tables 3 and 4 present the effect of scattering on the total radiative budgets of ground and space, for each cloudy configuration. Modification of ground total radiative budget due to scattering ranges from 1% to 6%, with a peak of 10% for the SAW middle cloud configuration. Statistical errors are never greater than 0.2%. As far as space is concerned (radiative flux toward space), scattering has a contribution of 1% to 5% over the total radiative budget, with error estimates below 0.1%.[3]

The fact that scattering should be considered as negligible or not, for long-wave atmospheric radiative transfer computations, depends entirely on the required accuracy level: for rough estimations, the absorption approximation is suitable; when a higher precision is required (1%), scattering should be taken into consideration.

5.2. Effects of scattering on NER and heating rates

Figs. 11 and 12 display the effect of scattering on the heating rates for MLS middle and high cloud configurations. These results have been computed as the differences of

---

[2] For instance ground and space radiative budgets need to be known with an uncertainty of less than one percent.

[3] These results are compatible with already published results (Fu et al., 1997); the purpose of this paper is not to present a strict comparison of results with other authors, and thus validate the analysis tool that we have developed. Its main purpose is rather to present a clear analysis of long-wave radiative transfers, in terms of Net Exchange Rates, concerning the role that scattering may play in terrestrial atmospheric long-wave radiative transfers.

Table 3
Effect of scattering on ground radiative budget

Configuration	Ψ_{ground} A.A. (W/m^2)	$\Delta\Psi_{ground}$ (W/m^2)	$\Delta\Psi_{ground}$ (%)
MLS low cloud	− 8.89	0.317 ± 0.005	− 3.57 ± 0.05
MLS middle cloud	− 29.45	0.788 ± 0.01	− 3.68 ± 0.05
MLS high cloud	− 69.73	0.743 ± 0.04	− 1.07 ± 0.06
MLS all clouds	− 8.89	0.325 ± 0.005	− 3.65 ± 0.05
SAW low cloud	2.51	− 0.16 ± 0.0009	− 6.27 ± 0.03
SAW middle cloud	− 1.07	0.11 ± 0.003	− 10.67 ± 0.2
SAW high cloud	− 71.00	2.38 ± 0.05	− 3.35 ± 0.07
SAW all clouds	− 2.51	− 0.12 ± 0.0009	− 5.00 ± 0.03

First column presents the cloud configuration. Second column presents the ground total radiative budget Ψ_{ground} in W/m^2 computed using the Absorption Approximation (A.A.) (Li and Fu, 2000). The third column presents the effect of scattering on ground total radiative budget $\Delta\Psi_{ground}$ in W/m^2 computed as the difference between the radiative budget taking into account scattering and the radiative budget with the absorption approximation. The reported uncertainties have been estimated from the Monte Carlo statistical standard deviations. The fourth column shows $\Delta\Psi_{ground}$ expressed in terms of percentage, with its statistical uncertainty.

NERs between a first computation for which scattering has been taken into account, and a second computation, for which scattering has been neglected (using the Absorption Approximation, see Fu et al., 1997). These results show that scattering mainly affects the clouds edges, and especially the top of the clouds. This effect is small for low and middle clouds: it is no higher than 2% of the absolute value of the heating rate at cloud edges (Fig. 11(a) compared to Fig. 7(a)). For those clouds, the effect of scattering is to decrease the absolute value of the heating rate at edges, i.e. to decrease the apparent absorption of the cloud.

For high and optically thin clouds, the effect of scattering on heating rate is not negligible and is as high as 10% at the cloud edges (Fig. 12(a) compared to Fig. 8(a)). In this configuration, scattering now increases the absolute value of the heating rate at cloud edges. However, scattering is still decreasing the absolute value of the total absorption by the cloud.

Let us try to understand these results, from simple considerations based on the following assumptions: radiation incident at the surface of clouds I will be assumed isotropic, no matter what are the sources. Clouds are also considered as isothermal,

Table 4
Same as Table 3 for space radiative budget

Configuration	Ψ_{space} A.A. (W/m^2)	$\Delta\Psi_{space}$ (W/m^2)	$\Delta\Psi_{space}$ (%)
MLS low cloud	286.71	− 4.12 ± 0.16	− 1.44 ± 0.05
MLS middle cloud	247.18	− 5.50 ± 0.10	− 2.22 ± 0.04
MLS high cloud	238.20	− 10.38 ± 0.17	− 4.36 ± 0.07
MLS all clouds	207.81	− 10.36 ± 0.11	− 4.99 ± 0.05
SAW low cloud	210.18	− 4.09 ± 0.10	− 1.95 ± 0.05
SAW middle cloud	200.25	− 4.63 ± 0.08	− 2.31 ± 0.04
SAW high cloud	182.04	− 7.74 ± 0.12	− 4.25 ± 0.06
SAW all clouds	176.52	− 8.37 ± 0.095	− 4.74 ± 0.05

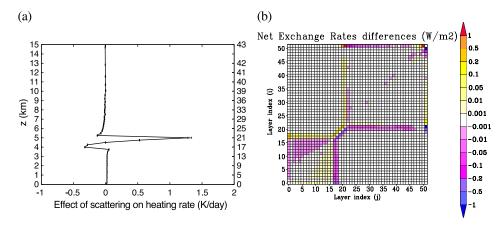(a)   (b)

Fig. 11. (a) Effect of scattering (mW/m^3) on MLS middle-cloud heating rates; (b) effect of scattering (W/m^2) on MLS middle-cloud NER matrix.

which is fairly well justified for radiative exchanges between a cloud and ground or space. Within these assumptions, the intensity of the exchange between radiative sources and the cloud is proportional to I, and its expression is given by Eq. (10) below:

$$I \int_{a}^{+\infty} [1 - \exp(-\kappa_a l)]p(l)dl \tag{10}$$

In the above equation, k_a is the absorption coefficient of the cloud and l is the length of scattering paths within the cloud. l is distributed according to the probability density function p on $[a, +\infty]$ where a is the smallest path length that can be encountered through the medium.

For a purely absorbing cloud ($k_s = 0$), the smallest path length within the cloud is $a = e$, where e is the cloud width. In this case, the cloud behaves as a blackbody at the optically thick limit for absorption ($k_a e \gg 1$).

If scattering is taken into account ($k_s \neq 0$), very small paths must be accounted for ($a = 0$). In this case, the cloud no longer behaves as a blackbody even for large k_a values. The mean path length $\langle l \rangle$ remains a constant no matter what are the scattering properties of the cloud (Blanco and Fournier, 2003), but the effect of scattering is to create a lot of short paths and some very long paths: scattering widens the path length distribution (increasing the standard deviation of l). In the case of optically thin clouds for absorption, this has no effect as $\int_{0}^{+\infty}[1 - \exp(-k_a l)]p(l)dl \approx k_a \langle l \rangle$ is constant when the cloud scattering properties change: for such clouds, scattering will not introduce any significant modifications of the cloud total radiative budget. However, for clouds which are not optically thin for absorption (which is the case most of the time for Earth configurations), convexity properties of the exponential function will result in a net
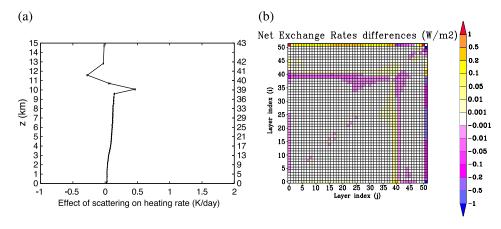
Fig 12. (a) Effect of scattering (mW/m^3) on MLS high-cloud heating rates; (b) effect of scattering (W/m^2) on MLS high-cloud NER matrix.

decrease of $\int_0^{+\infty}[1 - \exp(-k_a l)]p(l)\mathrm{d}l$, thus of the cloud total radiative budget. This is what was found for Earth cloudy configurations:

• For low (figure not shown) and middle cloud (Fig. 11) configurations, the cloud total radiative budget is negative, and scattering reduces its absolute value. The two maxima in the heating rate profile (at the bottom and at the top of the cloud) are both attenuated by scattering.
• For high cloud configurations (Fig. 12), the cloud total radiative budget is also negative. Even if scattering is to increase locally the heating rate peaks (radiative exchanges are concentrated at cloud edges), the heating rate at the top the cloud is more strongly attenuated than it is increased at the bottom of the cloud. This results in a net decrease of the absolute value of the cloud total radiative budget.

5.3. Spectral analysis

Fig. 13 represent the effect of scattering (mW/m^3/cm^1) on radiative budget $\Psi_{i,v}^{\text{total}}$ and its decomposition (net exchanges between each atmospheric layer and ground $\Psi_{i,v}^{\text{gas-ground}}$, between each atmospheric layer and space $\Psi_{i,v}^{\text{gas-space}}$, and between each atmospheric layer and the rest of the atmosphere $\Psi_{i,v}^{\text{gas-gas}}$) for an MLS middle-cloud configuration.

Conclusions about the effects of scattering on spectral heating rates are very similar to the previous results: scattering mainly modifies net exchanges between boundaries and cloudy layers. In low-cloud (figures not shown) and middle-cloud (Fig. 13) configurations, scattering decreases net exchanges between ground and cloudy layers, which means that photons emitted from the ground are backscattered by optically thick clouds; in high-cloud configurations (figures not shown), scattering mainly increases these net exchanges, which means that optically thin clouds do not significantly backscatter photons emitted from the ground; rather, photons do cross the cloud surface and scattering increases their mean path length, thus increasing the amount of energy absorbed by the cloud. Modifications occur
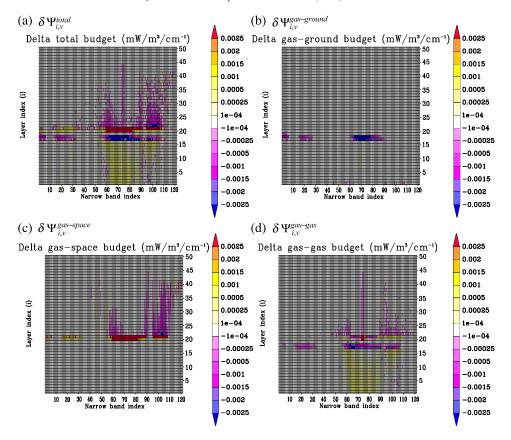
(a) $\delta \Psi_{i,v}^{total}$

(b) $\delta \Psi_{i,v}^{gas-ground}$

(c) $\delta \Psi_{i,v}^{gas-space}$

(d) $\delta \Psi_{i,v}^{gas-gas}$

Fig 13. (a) Effect of scattering on total radiative budget (mW/m^3/cm^1) as a function of narrow-band index (narrow-band width = 20 cm^{-1}, from 4 to 100 μm) and atmospheric layer index, for middle-cloud MLS configuration; (b) effect of scattering on net exchange between each atmospheric layer and ground (mW/m^3/cm^1); (c) effect of scattering on net exchange between each atmospheric layer and space (mW/m^3/cm^1); (d) effect of scattering on net exchange between each atmospheric layer and the rest of the atmosphere.

mainly in low absorption spectral regions, where exchanges between ground and cloudy layers are possible.

Similarly, scattering mainly modifies net exchanges between space and cloudy layers, as shown in Fig. 13(c), at frequencies where cloudy layers are visible from space. Scattering also brings a number of modifications to net exchanges between space and cloud-free atmospheric layers, in low absorption spectral regions.

Finally, scattering also affects gas–gas net exchanges, as seen on Fig. 13(d). Net exchanges between cloudy layers and the rest of the atmosphere are affected (because scattering will cause photons emitted into cloudy layers to lose more energy into the clouds, thus reducing net exchanges between these clouds and all other atmospheric layers); moreover, net exchanges between cloud-free layers and the rest of the atmosphere are also affected by scattering, mainly because of backscat-

tering by clouds: scattering will cause photons emitted in a given cloud-free layer to be backscattered by optically thick clouds, thus modifying all net-exchanges between the emitting layer and all atmospheric layers involved in the optical paths of the photons.

6. Summary and conclusions

The objective of this work is to analyze various simulation results concerning long-wave atmospheric radiative transfer. Radiative transfer computations have been carried out using a numerical algorithm based on a Monte-Carlo method developed in previous works (De Lataillade et al., 2002a; Eymet et al., 2004). Radiative transfer results have been expressed in terms of Net Exchange Rates (Green, 1967), allowing a more complete analysis of atmospheric long-wave heating rates (Cherkaoui et al., 1996, 1998). Results are presented for a number of configurations already used in a previous work from Fu et al., 1997.

A first series of results has been presented for clear-sky configurations; Net Exchange Rate matrices are presented, along with the corresponding long-wave atmospheric heating rates. Then radiative budget and its decomposition in terms of net exchanges between atmospheric layers and ground, net exchanges between atmospheric layers and space, and net exchanges between atmospheric layers and the rest of the atmosphere are shown, as a function of frequency and altitude. In a second part, the same results are shown for a series of cloudy atmospheres configurations; finally, the third part presents the effect of scattering over Net Exchanges Matrices, long-wave atmospheric heating rates and radiative budgets for cloudy atmospheres configurations.

In most of the atmosphere the radiative exchanges with boundaries (i.e. ground and space) represent more than 80% of the heating rate. The exchanges within the atmosphere play a significant role ($\approx$ 15% to 40% of the heating rate) only in the lower part of the atmosphere, just below the region where the optical thickness (computed from the top of the atmosphere) rises from optically thin to optically thick. The exchanges within the atmosphere may also be important to reduce vertical temperature gradient in the high atmosphere (Bresser et al., 1995) that may appear due to waves and which have not been considered here.

When thick clouds are present, the exchanges with boundaries (the cloud being considered as a boundary too) represent again the higher contribution to the radiative budget. Things are different with the high and thin clouds. They cannot be considered as boundaries and radiative exchanges may occur between atmospheric layers on both sides of the cloud.

In both low and high clouds, the effect of scattering by cloud droplets is to widen the photons path length distribution, thus decreasing the cloud total radiative budget. In the meantime, scattering may concentrate radiative net exchanges at cloud edges. Scattering appears to play a more important role for the flux at the top of atmosphere, the flux at the ground and the heating rate inside the cloud. The error on the flux at the top of the atmosphere may be as high as 10 W/m^2 whereas the error on the flux at the ground is

less important, except for very dry atmospheres, such as the Arctic profiles, for which both errors are of the same magnitude.

These results and their analysis in terms of Net Exchanges are intended to be used in the future for setting up a parameterization of long-wave radiative transfer for representation of the effects of scattering, in a terrestrial Global Circulation Model.

References

Blanco, S., Fournier, R., 2003. An invariance property of diffusive random walks. Europhysics Letter 61 (2), 168–173.

Bresser, G., Manning, A., Pawson, S., Rodgers, C.D., 1995. A new parametrization of scale-dependent radiative rates in the stratosphere. Journal of Atmospheric Sciences 52 n24, 4429–4447.

Cherkaoui, M., Dufrense, J.L., Fournier, R., Grandpeix, J.Y., Lahellec, A., 1996. Monte-Carlo simulation of radiation in gases with a narrow-band model and a net-exchange formulation. ASME Journal of Heat Transfer 118, 401–407.

Cherkaoui, M., Dufrense, J.L., Fournier, R., Grandpeix, J.Y., 1998. Radiative net exchange formulation within 1d gaz enclosures with reflective surfaces. ASME Journal of Heat Transfer 120, 275–278.

Clough, S.A., Iacono, M.J., 1995. Line-by-line calculation of atmospheric fluxes and cooling rates. 2—application to carbon dioxide, ozone, methane, nitrous oxide and the halocarbons. Journal of Geophysical Research 100 D8, 16519–16535.

De Lataillade, A., Dufrense, J.L., El Hafi, M., Eymet, V., Fournier, R., 2002a. A net exchange Monte Carlo approach to radiation in optically thick systems. Journal of Quantitative Spectroscopy and Radiative Transfer 74, 563–584.

De Lataillade, A., Blanco, S., Clergent, Y., Dufrense, J.L., El Hafi, M., Fournier, R., 2002b. Monte-Carlo method and estimations. Journal of Quantitative Spectroscopy and Relative Transfer 75, 529–538.

Dufresne, J.L., Gautier, C., Ricchiazzi, P., Fouquart, Y., 2002. Long-wave scattering effects of mineral aerosols. Journal of the Atmospheric Sciences 59, 1959–1966.

Dufresne, J.L., Hourdin, C., Fournier, R., Hourdin, F., Net exchange reformulation of radiative transfer in the CO_2 15 μm band on mars. To be submitted to Journal of Atmospheric Sciences.

Edwards, J.M., Slingo, S., 1996. Studies with a flexible new radiation code: 1. Choosing a configuration for a large-scale model. Quarterly Journal of the Royal Meteorolgical Society 122, 689–719.

Eymet, V., Fournier, R., Blanco, S., Dufrense, J.L., 2004. A boundary based net exchange Monte Carlo method for absorbing and scattering thick medium. Journal of Quantitative Spectroscopy and Radiative Transfer, accepted for publication.

Fels, S.B., Schwarzkopf, M.D., 1975. The simplified exchange approximation: a new method for radiative transfer calculations. Journal of Atmospheric Sciences 32, 1475–1488.

Fu, Q., Liou, K.N., Cribb, M.C., Charlock, T.P., Grossman, A., 1997. Multiple scatterring parameterization in thermal infrared radiative transfer. Journal of Atmospheric Sciences 54, 2799–2812.

Green, J.S.A., 1967. Division of radiative streams into internal transfer and cooling to space. Quarterly Journal of the Royal Meteorological Society 93, 371–372.

Hottel, H.C., Sarofim, A.F., 1967. Radiative Transfer. McGraw Hill, New York.

Joseph, J.M., Bursztyn, R., 1976. A radiative cooling model in the thermal infrared for application to models of the general circulation. Journal of Applied Meteorology 15, 319–325.

Lacis, A.A., Hansen, J.E., 1991. Description of the correlated-*k* distribution method for modeling nongray gaseous absorption, thermal emission, and multiple scattering in vertically inhomogeneous atmospheres. Journal of Geophysical Research 96, 9027–9063.

Lacis, A.A., Mishchenko, M.I., 1995. Climate forcing, climate sensitivity, and climate response: A radiative modeling perspective on atmospheric aerosols. In: Charlson, R.J., Heintzenberg, J. (Eds.), Aerosols Forcing of Climate, Environmental Sciences Research Report, vol. ES 17. J. Wiley, New York, pp. 11–42.

Li, J., Fu, Q., 2000. Absorption approximation with scatterring effect for infrared radiation. Journal of Atmo-spheric Sciences 57, 2905–2914.

Mc Clatchey, R.A., Fenn, R.W., Selby, J.E.A., Voltz, F.E., Garing, J.S., 1971. Optical properties of the atmosphere. Air Force Cambridge Research Laboratories Technical Report AFCRL-71-0279.

Rodgers, C.D., Walshaw, C.D., 1966. The computation of infrared cooling rate in planetary atmospheres. Quarterly Journal of the Royal Meteorological Society 92, 67–92.

Rothman, L.S., Barbe, A., Benner, D.C., Brown, L.R., Camy-Peyret, C., Carleer, M.R., Chance, K., Clerbaux, C., Dana, V., Devi, V.M., Fayt, A., Flaud, J.-M., Gamache, R.R., Goldman, A., Jacquemart, D., Jucks, K.W., Lafferty, W.J., Mandin, J.-Y., Massie, S.T., Nemtchinov, V., Newnham, D.A., Perrin, A., Rinsland, C.P., Schroeder, J., Smith, K.M., Smith, M.A.H., Tang, K., Toth, R.A., Auwera, V.J., Varanasi, P., Yoshimo, K., 2003. The hitran molecular spectroscopic database: edition of 2000 including updates of 2001. Journal of Quantitative Spectroscopy and Radiative Transfer 82, 1–4.

Schwarzkopf, M.D., Fels, S.B., 1991. The simplified exchange approximation revisited: an accurate, rapid method for computation of infrared cooling rates and fluxes. Journal of Geophysical Research 96, 9075–9096.

Stephens, G.L., 1984. The Parametrization of radiation for numerical weather prediction and climate models. Monthly Weather Review 112, 826–867.

Tessé, L., Dupoirieux, F., Zamuner, B., Taine, J., 2002. Radiative transfer in real gases using reciprocal and forward Monte Carlo methods and a correlated-k approach. International Journal of Heat and Mass Transfer 3 (13), 2797–2814.

Yang, S.R., Ricchiazzi, P., Gautier, C., 2000. Modified correlated k-distribution methods for remote sensing applications. Journal of Quantitative Spectroscopy and Radiative Transfer V64 (N6), 585–608.